# PLA-Derived Lactate Esters as Plasma Precursors for Hydrophilic and Antibacterial Coatings

Monika Strašáková[1], Eva Domincová Bergerová[1*], Marián Lehocký[1], Veronika Hanuliak[1], Hana Pištěková[1], Michal Urbánek[1], Pavel Sťahel[2], Monika Stupavská[2], Jakub Klaban[1], Anežka Lengálová[3], Vladimír Sedlařík[1]

[1]Centre of Polymer Systems, Tomas Bata University in Zlin, tr. Tomase Bati 5678, 760 01 Zlin, Czech Republic

[2] Department of Plasma Physics and Technology, Faculty of Science, Masaryk University, Kotlarska 267/2, 611 37 Brno, Czech Republic

[3] Faculty of Humanities, Tomas Bata University in Zlin, Stefanikova 5670, 760 01 Zlin, Czech Republic

[*]Correspondence: Eva Domincová Bergerová, domincova_bergerova@utb.cz

## Abstract

This study investigates the use of methyl lactate and ethyl lactate, prepared from virgin polylactic acid (PLA) through model chemical recycling, as bio-based precursors for atmospheric-pressure plasma deposition of multifunctional coatings on polyethylene terephthalate (PET). Plasma treatment significantly enhanced surface hydrophilicity, reducing the water contact angle from 76° for untreated PET to 27° for ethyl lactate and 51° for methyl lactate coatings. X-ray photoelectron spectroscopy (XPS) confirmed the incorporation of oxygen- and nitrogen-containing functional groups, while atomic force microscopy (AFM) and scanning electron microscopy (SEM) revealed surface morphology changes. The plasma-modified surfaces exhibited antibacterial activity against Escherichia coli and Staphylococcus aureus, achieving up to 3.4 and 2.3 log reductions, respectively, according to ISO 22196:2011. The results demonstrate the potential of lactate esters for hydrophilic and antibacterial plasma coatings and support future recycling-oriented and circular-economy-based plasma surface engineering approaches.

**Keywords:** Plasma deposition; surface modification; antibacterial coatings; lactate esters; polyethylene terephthalate; circular economy

## Introduction

Plastics have become some of the most widely produced and utilized materials globally. The substantial growth in production and consumption has led to the accumulation of large quantities of waste, presenting a significant challenge for environmentally responsible disposal. Projections suggest that annual global production will result in approximately 12,000 Mt of waste by 2050. As production continues to rise, the resulting excess waste poses an increasing environmental threat to both humanity and the planet. Traditional waste management methods, such as landfilling, are inadequate due to the non-biodegradable nature of many conventional polymers, which leads to their prolonged persistence in disposal sites [1,2].

In response to this issue, there has been growing interest in alternative materials that retain the functional properties of conventional materials while being more environmentally sustainable. This has spurred the development of biodegradable polymers, now used in the production of eco-friendly alternatives. Bio-based polymers, aligned with the principles of sustainable production and consumption, have emerged as key materials in this context [1,3]. The demand for bioplastics has surged as a viable alternative to traditional polymers, primarily due to their renewable nature, non-toxicity, biodegradability, and biocompatibility. Furthermore, modern bio-based materials exhibit mechanical properties that are comparable to those of their fossil-derived counterparts [4].

Among the various bioplastics, polylactic acid (PLA) is considered one of the most promising candidates for replacing non-degradable polymers such as polyethylene terephthalate (PET) and polystyrene (PS), particularly in food packaging applications. However, the increasing production and use of PLA, combined with inadequate consumer waste collection systems and limited technological solutions for its effective recycling, have resulted in frequent cross-contamination of recycling streams. In practice, potential future valorisation of PLA waste is often unintentionally mixed with conventional plastic waste, most notably with PET recycling streams, where even small amounts of PLA can negatively affect the recycling process and the quality of recycled PET. Consequently, the simultaneous management of biodegradable and non-biodegradable plastics within the same waste management infrastructure remains a significant challenge [5,6].

A promising approach to this issue is processing of waste materials, which involves a systematic technological approach and the repurposing of waste. For PLA, potential processing waste routes include landfilling or composting, incineration, and both mechanical and chemical

recycling. However, these methods pose several challenges, including the loss of valuable polyhydroxy acids, degradation of soil quality, and the release of toxic exhaust gases.

In contrast, chemical recycling represents a promising strategy for extending the lifecycle of post-consumer plastic waste. In the case of PLA, chemical recycling is considered an economically viable and environmentally sustainable approach, as it enables the depolymerization of the ester backbone into valuable low-molecular-weight compounds, primarily lactate esters, which can be further utilized as functional precursors in various applications [3]. An important advancement in surface engineering is plasma polymerization, a process in which reactive species generated in the plasma phase - such as radicals, ions, and excited molecules - are formed from a gaseous precursor and subsequently deposited onto a substrate, where they recombine to form a highly cross-linked polymer-like thin film [7]. Plasma-based technologies offer several advantages, including solvent-free processing, low thermal load, and reduced use of hazardous chemicals. Importantly, plasma treatment modifies only the surface of a material while preserving its bulk properties. In addition, plasma exposure can introduce polar functional groups, such as hydroxyl and carboxyl moieties, which significantly enhance surface wettability, as evidenced by the reduction in water contact angle following treatment [8].

However, further research is needed on the plasma processing of PLA esters, such as ethyl lactate and methyl lactate, which are decomposition products resulting from chemical recycling. Furthermore, existing literature largely focuses on the combination of commercially available ethyl lactate with additives, nanoparticles, or composites, rather than exploring plasma deposition or polymerization of PLA decomposition products [9–11].

This study investigates the application of plasma technology in the processing of products derived from the chemical recycling of biopolymers, with a focus on optimizing ecological sustainability. By integrating these approaches, this work not only offers a sustainable solution for addressing the projected accumulation of plastic waste by 2050 but also produces materials with enhanced properties suitable for a wide range of applications, marking a significant step forward in the implementation of circular economy practices and the development of sustainable materials.

Considering the need for more sustainable valorization routes for chemically recycled PLA monomers and the scarcity of studies on their plasma-assisted deposition, there is a clear research gap. Moreover, PET is one of the most common non-biodegradable packaging

materials and provides an ideal substrate for surface modification, where tailored coatings can impart new functionalities without altering bulk properties.

Therefore, the aim of this study is to investigate the plasma-assisted deposition of methyl lactate and ethyl lactate obtained through chemical recycling of PLA onto PET substrates under atmospheric pressure conditions. The work focuses on (i) characterizing the chemical composition and morphology of the deposited layers, (ii) evaluating their hydrophilic properties, and (iii) assessing their antibacterial performance. By linking model chemically recycled PLA-derived compounds after the solvolysis process with plasma deposition, this work establishes a link between chemical recycling of biopolymers and plasma surface engineering by demonstrating that methyl and ethyl lactate obtained from PLA can serve as effective precursors for the preparation of hydrophilic and antibacterial coatings on PET substrates.

## Materials and methods

### 1.1 Materials

Polyethylene terephthalate (PET) films (TFP universal a.s., Dobřejovice, Czech Republic) with dimensions of 120 mm × 1000 mm and a thickness of 1 mm were used as substrates for deposition and served as a reference material. The monomers utilized for plasma deposition were ethyl lactate and methyl lactate, prepared from virgin PLA (Ingeo™ 2003D, NatureWorks®, Minneapolis, USA), through controlled solvolysis reactions and used as model compounds for future recycling-oriented plasma processing applications. The product purity (≥ 98%) was determined as described by Domincova Bergerova et al. [12]. The bacterial strains *Staphylococcus aureus* (CCM 4516) and *Escherichia coli* (CCM 4517) were sourced from the Czech Collection of Microorganisms, Masaryk University (Brno, Czech Republic).

### 1.2 Sample preparation - plasma deposition

Plasma deposition was conducted according to Šťahel et al. [13], with a few minor adjustments. PET films were prepared and served as the initial substrates for plasma deposition. Thin film plasma polymerization was performed in a specially designed reactor equipped with a surface dielectric barrier discharge (SDBD) system. The reactor comprised three primary components: an electrode system, a cooling system, and a high-voltage generator. The complete deposition

apparatus was situated within a fume hood throughout the deposition procedure, and the resultant gaseous products were continuously evacuated. The SDBD electrode setup consisted of 11 upper rotating cylindrical brass electrodes with a diameter of 1 cm and a length of 10.4 cm, spaced 2 mm apart. Below the cylindrical electrodes, a flat lower electrode of the size of 13.6 x 10 cm was positioned and covered with a 1 mm thick mica dielectric. The substrate was periodically moved along the upper and lower electrodes at a speed of 3 cm/min. As the upper electrodes rotated, they contacted the moving substrate. The lower electrode was grounded, whereas the upper electrodes were connected to a high-voltage AC power supply (Lifetech, Brno, Czech Republic) using a sinusoidal voltage with an amplitude of 11 kV and a frequency of 12 kHz. The power input to the system was set to 150 W. A schematic of the experimental setup is presented in Fig. 1. A summary of the main plasma deposition parameters used in the present study is provided in Table S1 in the Supplementary Information.

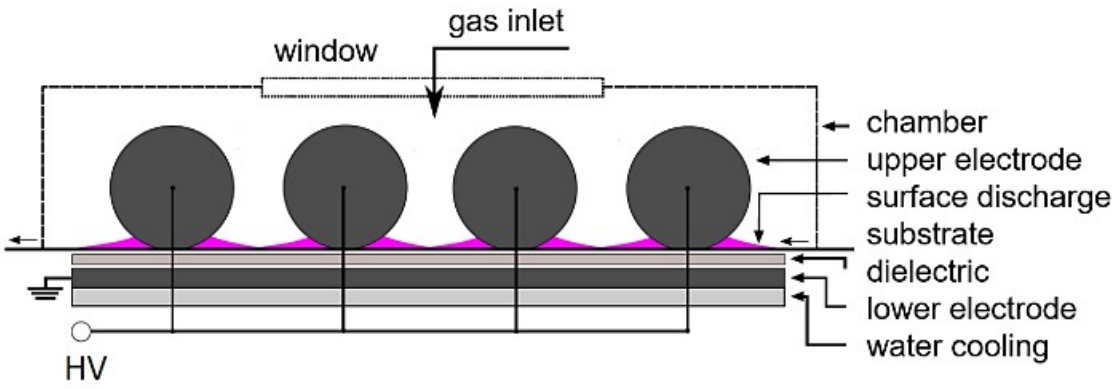


Figure 1: Schematic of the deposition setup [13].

As the working gas, nitrogen was used; it was supplied between the upper electrodes at a flow rate of 3 slm. The monomers ethyl lactate and methyl lactate as precursors were introduced into the nitrogen flow at rates ranging from 250 to 1000 sccm. The substrate passed through the discharge three times, with a total deposition time of 6.5 seconds. Throughout the deposition process, the apparatus was water-cooled to maintain a consistent electrode temperature.

## 2.3 Characterization of chemical structure

### 2.3.1 Fourier transform infrared spectroscopy with attenuated total reflection

Fourier transform infrared spectroscopy with attenuated total reflection (ATR-FTIR) spectra were recorded for all polymer films using a Nicolet iS5 spectrometer (Thermo Fisher Scientific,

Waltham, USA), equipped with a Ge crystal. The analysis was conducted over a range of 600–4000 $cm^{-1}$ with a resolution of 4 $cm^{-1}$, and 64 scans were averaged per spectrum. Data processing was performed using OMNIC software (Thermo Fisher Scientific, Waltham, USA).

### 2.3.2 X-ray photoelectron spectroscopy

X-ray photoelectron spectroscopy (XPS) analysis was conducted using an ESCALAB 250Xi system (Thermo Fisher Scientific, East Grinstead, UK), utilizing an X-ray beam with a power output of 200 W and a spot size of 650 microns. Survey spectra were collected with a pass energy of 50 eV and an energy step of 1 eV, while high-resolution scans were performed with a pass energy of 20 eV and an energy step of 0.1 eV. To mitigate surface charging effects, an electron flood gun was employed. All spectra were referenced to the C1s hydrocarbon component with a binding energy of 284.8 eV. Data calibration, processing, and fitting were performed with Avantage software (version 5.9925).

### 2.3.3 Spectroscopic ellipsometry

The thickness of selected plasma-polymerized coatings was determined using a HORIBA UVISEL 2 spectroscopic ellipsometer (HORIBA Scientific, France). Measurements were performed at an angle of incidence of 70° in the spectral range of 250–1000 nm. The spectra were acquired with a wavelength step of 2 nm, using an integration time of 400 ms. The measurement spot size was 2030 × 705 µm. The experimental $\Psi$ and $\Delta$ spectra were analysed using an optical model consisting of a PET substrate and a plasma-polymerized surface layer. Coating thicknesses were obtained by fitting the model to the measured data. The goodness of fit was evaluated using the $\chi^2$ statistic, which quantifies the agreement between the experimental data and the fitted optical model.

## 2.4 Characterization of hydrophilic properties

The wettability of the sample surface was evaluated by measuring the static contact angle (CA) using a SEE System instrument (Advex Instruments, Czech Republic), equipped with a UVC camera and a high-resolution glass objective lens. Three test liquids were employed: ultrapure water (resistivity 18.2 MΩ·cm, Milli-Q, Merck), diiodomethane (≥99%, Sigma Aldrich), and ethylene glycol (≥99%, Sigma Aldrich). Droplets of 3 µL were deposited on the surface using a micropipette, and images were acquired approximately 1 s after deposition. For each liquid and sample, five independent measurements were performed, and the average values are reported. The images were analyzed using the SEE System software to determine the contact angle. The standard deviations were calculated according to the Dean–Dixon approach for small

data sets, which is suitable for a limited number of repeated measurements (n = 5). The total surface free energy (γ^tot) and its dispersive (γ^d) and polar (γ^p) components were calculated according to the **Owens–Wendt–Rabel–Kaelble (OWRK) method** [14], using the following relationship (1):

$$\gamma_L(1 + \cos\theta) = 2\left(\sqrt{\gamma_S^d \gamma_L^d} + \sqrt{\gamma_S^p \gamma_L^p}\right) \quad (1)$$

where θ is the measured contact angle, $\gamma_L$ is the surface tension of the liquid and $\gamma_S$ is the surface free energy of the solid. Superscripts d and p denote dispersive and polar components, respectively. The surface tension parameters of the test liquids used for the OWRK calculation were taken from literature [14] and provided in Table S2 in the Supplementary Information.

## 2.5 Characterization of morphology

### 2.5.1 Scanning electron microscopy

Scanning electron microscopy (SEM) images of the sample surfaces and fracture areas were obtained using a Nova NanoSEM 450 (FEI, USA). Prior to imaging, the samples were coated with a gold–palladium alloy to improve electrical conductivity; the coating was deposited by sputtering, which lasted 60 s and resulted in the film thickness of approximately 10 nm, with a grain size in the range of 3–5 nm. The SEM measurements were conducted at a working distance (WD) of 4.7 mm and an accelerating voltage (HV) of 5 kV.

### 2.5.2 Atomic force microscopy

The surface topography of treated and untreated PET films was characterized using an atomic force microscope (AFM) model Dimension-Icon. Measurements were conducted at a scan rate of 1 Hz with a resolution of 256 × 256 pixels in tapping mode under ambient air conditions. For the measurements, a silicon-nitride probe ScanAsyst-Air (both Bruker, Billerica, MA, USA) with a resonant frequency of 70 kHz and a stiffness constant of 0.4 $N \cdot m^{-1}$ was employed.

## 2.6 Characterization of antibacterial properties

The antibacterial properties of the samples were evaluated following the ISO 22196:2011 standard. Prior to testing, the samples were disinfected with 70% denatured ethanol. Bacterial suspensions of *E. coli* ($3.1 \times 10^5$ $CFU \cdot mL^{-1}$) and *S. aureus* ($4.0 \times 10^5$ $CFU \cdot mL^{-1}$) were prepared in 1/500 nutrient broth (HiMedia laboratories, Mumbai, India). A 100 µL aliquot of bacterial suspension was applied to the surface of the samples (25 × 25 mm), which were then covered with polypropylene foil (20 × 20 mm). Afterwards, the samples were incubated at 35 °C and

100% relative humidity for 24 hours. Following incubation, the polypropylene foil was removed, and the samples were washed with soya casein digest lecithin polysorbate broth, which was subsequently collected. Antibacterial experiments were performed in triplicate, and the results are reported as mean ± standard deviation. For aging evaluation, the coated samples were stored under laboratory ambient conditions for one year and subsequently re-tested using the same antibacterial testing procedure described above.

The antibacterial activity was evaluated using equation (2):

$$R = U_t - A_t \quad (2)$$

where $R$ is the antibacterial activity, $U_t$ means the common logarithm of the viable bacteria count ($CFU \cdot cm^{-2}$) recovered from the untreated (blank) sample, and $A_t$ stands for the count for the treated specimen after 24 hours [15].

For subsequent analyses, the plasma-treated samples at a flow rate of 1000 sccm were used.

## 3 Results and discussion

### 3.1 Characterization of chemical structure

#### 3.1.1 ATR-FTIR Analysis

As seen in Figure 2, the ATR-FTIR spectra of all samples, including methyl lactate/PET, ethyl lactate/PET, and bare PET, exhibit near-identical profiles. Comparison of the spectra using the OMNIC software library revealed a greater than 99% match for all samples. Notably, the ethyl lactate/PET and the methyl lactate/PET samples exhibited changes in the region between 3500 and 2600 $cm^{-1}$, corresponding to O-H or N-H bonds, which may contribute to increased hydrophilicity [16]. The spectral similarity suggests that the deposited plasma films are relatively thin, with the FTIR signal predominantly influenced by the underlying PET substrate. Moreover, as no previous studies have reported FTIR spectra for plasma-treated ethyl lactate and methyl lactate, this aspect remains insufficiently understood and warrants further systematic investigation.

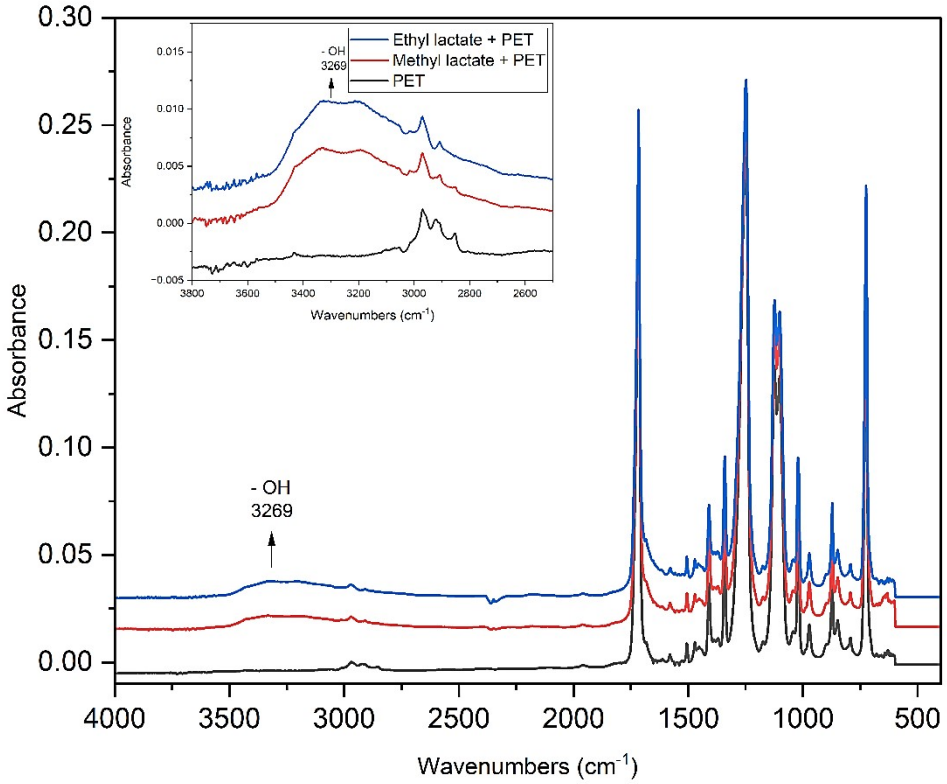


Figure 2: FTIR spectra of samples: methyl lactate/PET (flow rate 1000 sccm), ethyl lactate/PET (flow rate 1000 sccm) and bare PET.

### 3.1.2 Surface composition of samples

The surface composition of samples was followed with X-ray photoelectron spectroscopy and the results are summarized in Table 1. As can be seen, the reference PET sample exhibits 74% carbon and 24% oxygen, which is consistent with theoretical expectations [17]. The O/C ratio, indicative of increased surface oxygen-containing functionalities, is 0.324. For the plasma-modified methyl lactate/PET sample, the surface consists of 61% carbon, 27% oxygen, and 11% nitrogen, resulting in an increased O/C ratio of 0.443. In the case of the ethyl lactate/PET sample, nitrogen content was markedly higher reaching 25%, with oxygen also present at 25%, and carbon at 50%. The O/C ratio for this sample is 0.5, representing an over 1.5-fold increase compared to the reference PET sample. These results indicate substantial surface functionalization following plasma deposition.

Table 1 Sample elemental surface composition (%) and bond distributions (%) according to XPS analysis. Samples: methyl lactate/PET (flow rate 1000 sccm), ethyl lactate/PET (flow rate 1000 sccm) and bare PET.

| | | PET reference (%) | methyl lactate/PET (%) | ethyl lactate/PET (%) |
|---|---|---|---|---|
| | **C** | 74 | 61 | 50 |
| | **O** | 24 | 27 | 25 |
| | **N** | 0 | 11 | 25 |
| **C1s** | **C=C** | 15 | 11 | 6 |
| | **C-C/C-H** | 50 | 45 | 28 |
| | **C-N** | 0 | 8 | 13 |
| | **C-O** | 23 | 13 | 10 |
| | **C=O** | 0 | 2 | 8 |
| | **N-C=O** | 0 | 3 | 10 |
| | **COO** | 12 | 18 | 25 |
| **N1s** | **-C=N** | - | 5 | 5 |
| | **-C-NH-** | - | 69 | 57 |
| | **-CONH-** | - | 16 | 30 |
| | **nitrate** | - | 10 | 8 |

The formation of oxygen- and nitrogen-containing functionalities can be explained by fragmentation–recombination processes occurring during plasma polymerization in the nitrogen SDBD discharge. Under atmospheric-pressure plasma conditions, energetic electrons, ions, metastable nitrogen species, and UV radiation induce extensive fragmentation of methyl lactate and ethyl lactate molecules through cleavage of ester C–O, C–C, and O–H bonds. This process generates a broad spectrum of reactive radicals and molecular fragments containing carbonyl, alkoxy, hydroxyl, and hydrocarbon moieties. Simultaneously, the nitrogen plasma produces reactive nitrogen species (RNS), including excited nitrogen molecules, nitrogen radicals, and ionic species. Subsequent recombination reactions in the plasma phase and at the substrate surface led to the formation of highly cross-linked plasma-polymerized layers enriched with oxygen- and nitrogen-containing functional groups. The incorporation of nitrogen-containing functionalities detected by XPS, including C–N, N–C=O, and amine-related groups, likely results from reactions between precursor-derived radicals and reactive

nitrogen plasma species. Similar fragmentation and recombination pathways have been described for plasma polymerization of oxygen-containing organic precursors under atmospheric-pressure dielectric barrier discharge conditions [18],[19].

For a more detailed analysis of the effect of plasma modification, high-resolution XPS spectra of the C1s and N1s were measured (Figure 3). The figure reveals distinct differences in surface chemistry between the reference PET and the plasma-modified samples, with variations also observed between the methyl and ethyl lactate treatments. Deconvolution of these spectra provided further insights into the formation of oxygen- and nitrogen-containing functional groups generated during plasma polymerization.

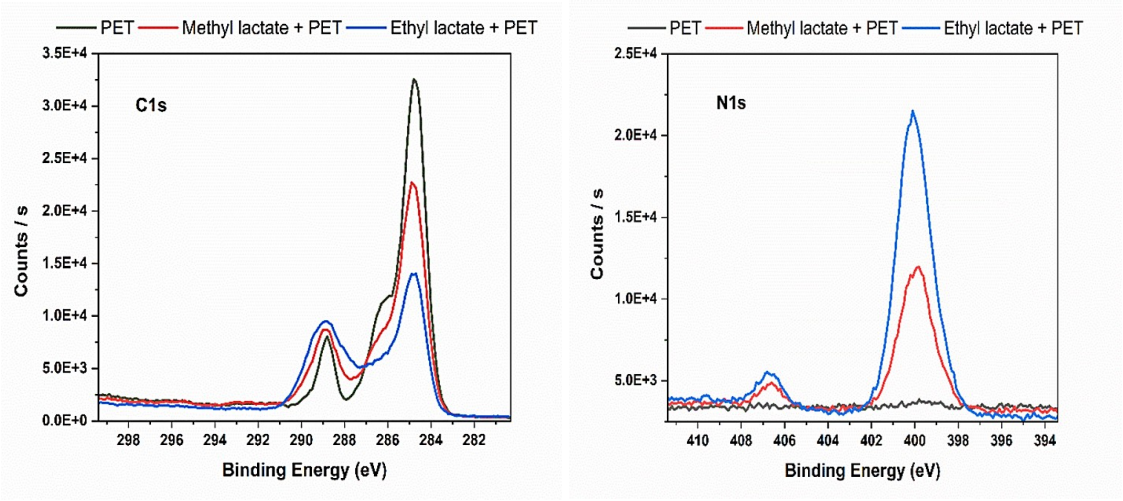


Figure 3: Overlay of XPS C1s and N1s spectra of the PET reference and plasma modified samples (methyl lactate/PET and ethyl lactate/PET).

The C1s spectra of the reference PET sample were deconvoluted into four distinct peaks with binding energies of 284.5 eV, 284.8 eV, 286.4 eV, and 289 eV, corresponding to carbon atoms in C=C, C–C/C–H, C–O, and COO functional groups, respectively. Following plasma modification, three additional peaks emerged at binding energies of 285.7 eV, 287.7 eV, and 288.4 eV, which are assigned to C–N, C=O, and N–C=O functional groups, respectively (Figure 4) [20],[21], [22],[23],[24] . The relative concentrations of all detected carbon functional groups on the surface of the analyzed samples are presented above in Table 1. The incorporation of nitrogen-containing groups is particularly noteworthy, given that nitrogen was used as the carrier gas. Under plasma conditions, nitrogen molecules are activated into reactive species, which can readily react with carbon-centered fragments originating from the precursor. This leads to the formation of C–N, amide-like (N–C=O), and imine-related structures, indicating

that the final surface chemistry is governed not only by the precursor composition but also by plasma-phase reactions involving the working gas.

Deconvolution of the C1s spectra reveals a progressive reduction in the relative contributions of nonpolar carbon environments (C=C and C–C/C–H) compared to the reference PET. The fraction of C=C bonds decrease from 15% in pristine PET to 11% in methyl lactate/PET and to 6% in ethyl lactate/PET, while C–C/C–H bonds drop from 50% to 45% and 28%, respectively. Importantly, this decrease does not indicate chemical consumption or transformation of the aromatic structures of PET. Rather, it reflects attenuation of the XPS signal from the underlying polymer due to coverage by a thin plasma-deposited film. Because XPS probes only the outermost nanometers of the surface, the detected bonding environment primarily represents the newly formed coating rather than the bulk PET substrate. This interpretation is further supported by the simultaneous increase in polar functional groups, including C–O, C=O, and N –C=O, which collectively indicate the formation of a heteroatom-rich surface. The COO contribution rises from 12% in the reference PET to 18% in methyl lactate/PET and 25% in ethyl lactate/PET, while C–N and N–C=O functionalities are absent in pristine PET but clearly present in both modified samples. These changes confirm that plasma-assisted deposition introduces a highly functionalized surface layer enriched in ester, carbonyl, amide, and amine-related structures. From a functional perspective, the increased abundance of carbonyl- and nitrogen-containing groups is directly linked to enhanced surface polarity. Carbonyl groups contribute to dipole–dipole interactions, while amine and amide functionalities can act as hydrogen bond donors and acceptors. These chemical features provide a molecular-level explanation for the observed increase in surface free energy and the pronounced decrease in water contact angle, particularly for the ethyl lactate-derived coating.

The N1s spectra further support this interpretation. The plasma-treated samples display peaks corresponding to imine (-C=N, 398.6 eV), amine (-C-NH-, 400 eV), amide (-CONH-, 401.0 eV), and nitrate ($NO_3^-$, 406.7 eV) functionalities (Figure 5). Nitrogen is incorporated predominantly in the form of amine groups, which represent the major nitrogen species in both ester-derived coatings. This suggests that recombination pathways favor the formation of reduced nitrogen functionalities, likely due to the high reactivity of hydrogen-containing fragments in the plasma phase.

The presence of amide groups indicates that reactions between nitrogen species and oxygen-containing fragments (e.g., carbonyl groups derived from the precursor) are also significant. This points to a complex interplay between fragmentation and recombination processes, leading

to the formation of multifunctional surface chemistry. The signal attributed to oxidized nitrogen species is relatively minor and is tentatively assigned to nitrate-like groups, which may originate from post-plasma oxidation upon exposure to ambient air. Such contributions are commonly reported in plasma-treated polymer systems and should be interpreted with caution [18].

The significantly higher nitrogen incorporation observed for ethyl lactate/PET compared to methyl lactate/PET may be associated with differences in precursor molecular structure and plasma fragmentation behavior. Ethyl lactate contains a longer ethyl substituent, which may favor the formation of more stable carbon-centered radicals and hydrocarbon fragments during plasma activation. These intermediates can more effectively participate in recombination reactions with reactive nitrogen species generated in the nitrogen discharge, thereby promoting the incorporation of amine- and amide-related functionalities into the deposited coating. In contrast, methyl lactate, owing to its lower molecular weight and simpler structure, is expected to undergo more extensive fragmentation and volatilization under plasma conditions, which may limit the formation and retention of nitrogen-containing surface species. Similar precursor-dependent variations in plasma polymer chemistry have been reported for atmospheric-pressure plasma polymerization of oxygen-containing organic compounds [18], [19].

The XPS results confirm successful plasma-assisted deposition of ester-derived coatings onto PET. The observed spectral changes are governed by the formation of a new, thin, heteroatom-rich surface layer that masks the underlying PET signal, rather than by chemical modification of the PET backbone itself. The surface chemistry is governed by plasma-induced fragmentation–recombination processes and is strongly influenced by plasma reactions rather than preserving the original molecular structure of the precursors. This distinction is essential for interpreting XPS data of plasma polymers and for understanding the relationship between processing conditions, surface chemistry, and functional properties. Overall, the observed surface chemical changes are consistent with the enhanced hydrophilicity and confirm the formation of a highly functionalized, highly cross-linked, and chemically heterogeneous plasma-polymerized surface layer.

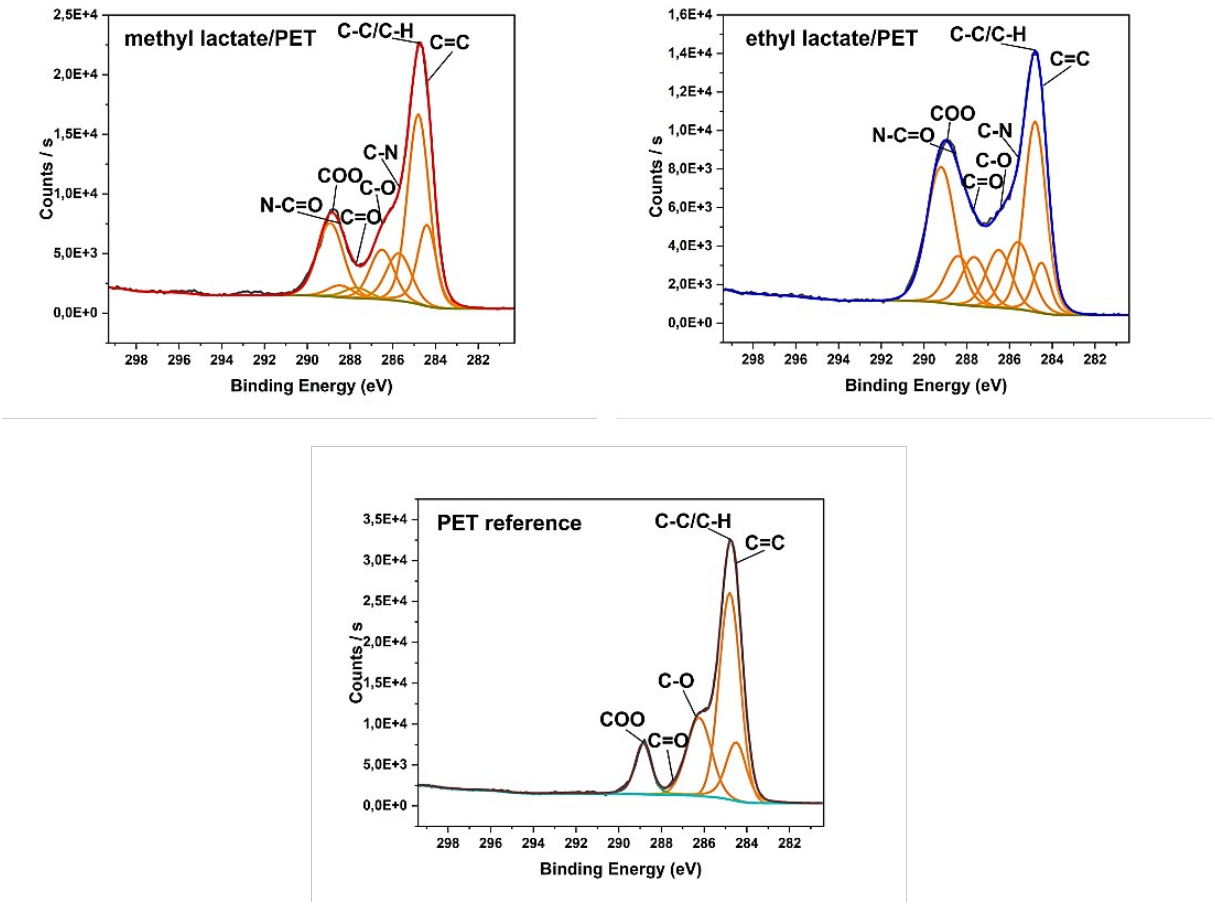


Figure 4: High-resolution XPS C1s spectra of the untreated PET reference and plasma-modified methyl lactate/PET and ethyl lactate/PET samples, including peak deconvolution and assignment of individual carbon-containing functional groups.

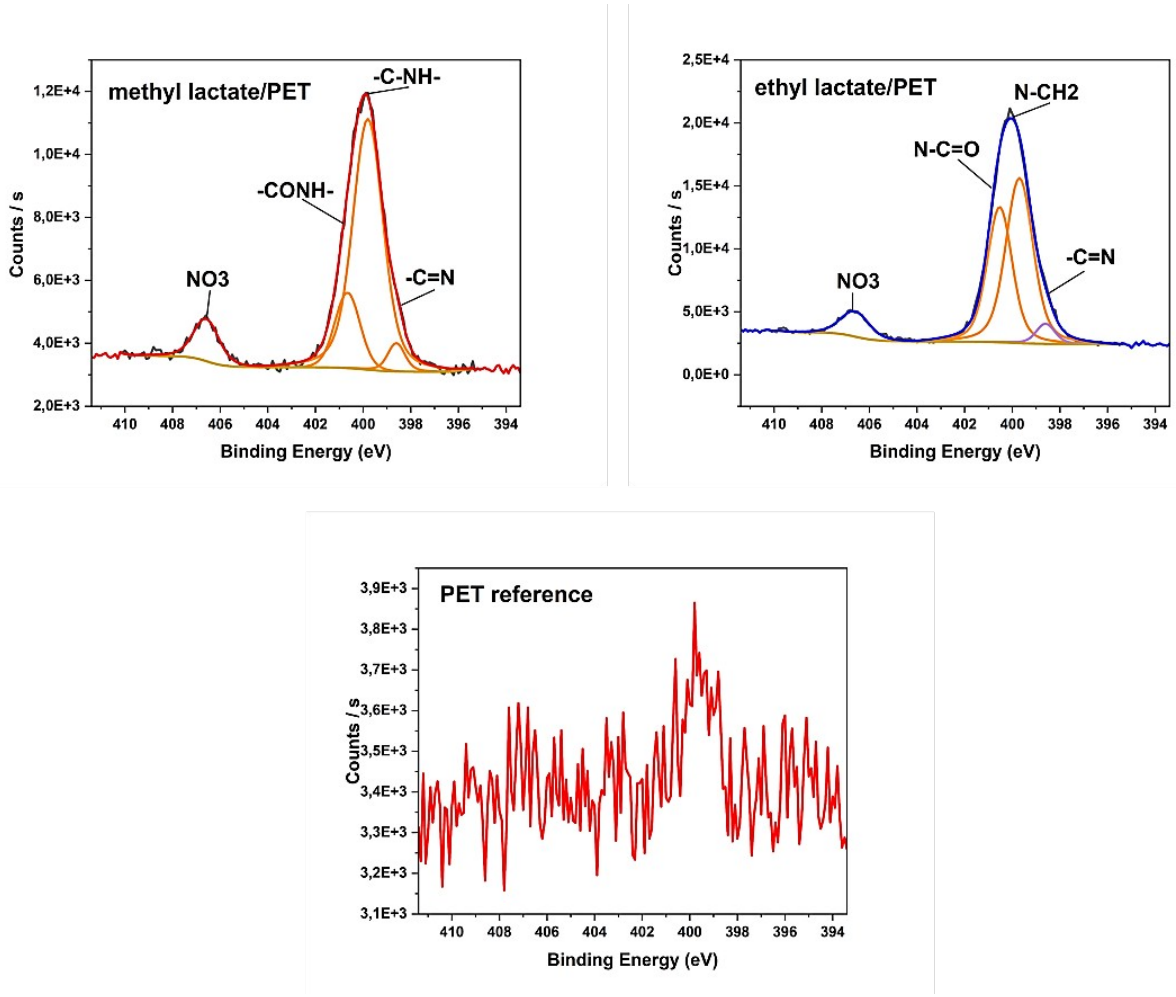


Figure 5: High-resolution XPS N1s spectra of the untreated PET reference and plasma-modified methyl lactate/PET and ethyl lactate/PET samples, including peak deconvolution and assignment of nitrogen-containing functional groups.

3.1.3 Coating thickness determination

Direct coating thickness measurements were performed using spectroscopic ellipsometry and the results are summarized in Table 2.

Table 2 Thickness of plasma-polymerized coatings deposited on PET substrates.

| Sample | Flow Rate (sccm) | layer thickness (nm) | $\chi^2$ |
|---|---|---|---|
| 1. ethyl lactate | 500 | 59.8 ± 0.4 | 0.98 |
| 2. ethyl lactate | 1000 | 92.8 ± 1.6 | 1.23 |
| 3. methyl lactate | 500 | 71.5 ± 3.0 | 6.67 |
| 4. methyl lactate | 1000 | 88.7 ± 1.6 | 0.91 |

The untreated PET reference sample was analysed using the same optical model, yielding an apparent surface-layer thickness of approximately 100 nm and thereby confirming the applicability of the fitting procedure. The obtained value reflects the optical response of the PET substrate within the applied model and is reported only as a reference; it does not correspond to a plasma-polymerized coating.

The deposited plasma-polymerized layers exhibited thicknesses ranging from approximately 60 to 93 nm. For both precursor systems, increasing the precursor flow rate resulted in thicker coatings. These results confirm the successful formation of thin plasma-polymerized layers on the PET surface and support the interpretation of the ATR-FTIR and XPS analyses, which indicated the presence of relatively thin deposited coatings.

The obtained $\chi^2$ values indicate good agreement between the experimental data and the applied optical model. Representative ellipsometric fitting curves are provided in the Supplementary Information (Figures S1–S4).

### 3.2 Hydrophilicity of materials - contact angle and surface energy evaluation

The contact angle (CA) values and calculated surface free energy (SFE) of the samples are summarized in Table 3. Water CA values serve as a qualitative indicator of hydrophilic versus hydrophobic character, whereas the complete set of contact angles obtained with different probe liquids is required for quantitative SFE analysis.

As shown in Table 3, plasma modification progressively enhanced the hydrophilic properties of both ethyl lactate and methyl lactate coatings. For ethyl lactate, the most pronounced hydrophilicity was observed at a monomer flow rate of 1000 sccm, with a water CA of 27 ± 2°. In contrast, the lowest CA achieved for methyl lactate under the same conditions was 51 ± 3°. These results indicate that ethyl lactate plasma layers introduce a higher density of polar functionalities than methyl lactate, consistent with XPS findings that revealed greater incorporation of oxygen- and nitrogen-containing groups. Such a pronounced difference in wettability is particularly relevant, as previous studies have shown that only surfaces with very low water contact angles (below ~30°) are capable of sustaining stable hydration layers that effectively alter interfacial interactions [25,26]. The evolution of water CA values for both coatings is presented graphically in Figure 6.

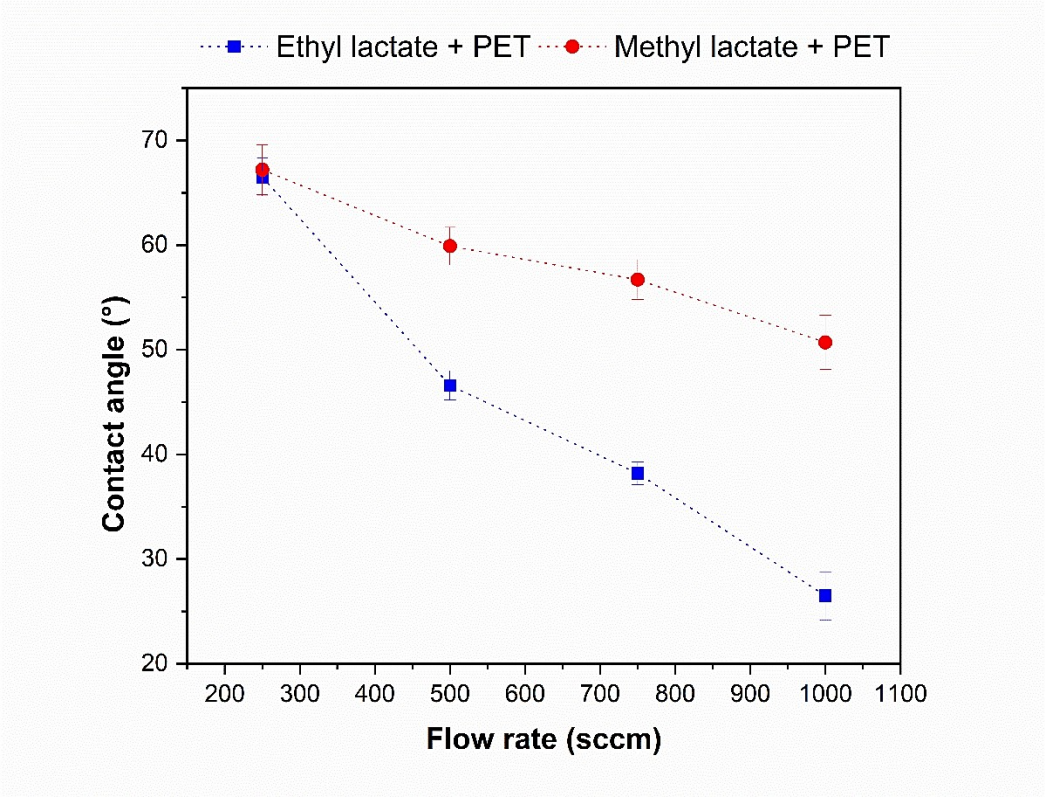


Figure 6: Water contact angle values for plasma-polymerized ethyl lactate/PET and methyl lactate/PET films. Error bars represent standard deviation obtained from five independent measurements (n = 5).

The Owens–Wendt analysis further confirmed that plasma treatment predominantly increased the polar contribution (γ^p) of SFE, while the dispersive part (γ^d) remained nearly unchanged. For example, ethyl lactate at 1000 sccm exhibited a total SFE of 60 $mJ \cdot m^{-2}$ with a dominant polar fraction, compared to only 46 $mJ \cdot m^{-2}$ for untreated PET. This trend is supported by XPS (Table 1), which detected incorporation of polar oxygen- and nitrogen-containing groups (–OH, –C=O, –C–N, N–C=O). Importantly, FTIR spectroscopy (Figure 2) provided complementary evidence, revealing a more pronounced presence of –OH functionalities in ethyl lactate compared to methyl lactate coatings. In sum, the XPS and FTIR results suggest that plasma deposition promotes the incorporation of hydroxyl and nitrogen-containing groups, which may contribute to the enhanced surface polarity and hydrophilicity.

Comparable trends have been documented for other plasma-modified polymers. Lai et al. demonstrated that plasma treatment of polymers results in a significant decrease in water CA and a corresponding increase in SFE, primarily due to oxygen incorporation [27]. Johnston and Ratner reported that plasma-polymerized organic films exhibit a marked increase in γ^p following the introduction of heteroatom-containing moieties [28], while Cui and Brown

showed that in plasma-treated polypropylene the rise in SFE is attributable predominantly to γ^p [29]. More recent work corroborates these findings, including the deposition of nanocomposite coatings from ethyl lactate [29] and rapid hydrophilization via atmospheric plasma polymerization [30].

Analogous effects of plasma treatment on the enhancement of surface polarity and wettability have also been reported for polycarbonate [31], PET films modified by plasma-based ion implantation [32], and PET track membranes [33], underlining the universal nature of plasma-induced hydrophilization across diverse polymeric systems.

Overall, both the present data (Table 3) and the literature suggest that the observed hydrophilization of PET surfaces coated with plasma-polymerized lactate esters originates from the introduction of polar functional groups, particularly hydroxyl and nitrogen species, leading to an increase in γ^p that clearly outweighs changes in dispersive interactions.

Table 3 Contact angles of plasma-polymerized films deposited at different monomer flow rates. The PET reference represents the untreated substrate. Values are presented as mean ± standard deviation (n = 5).

| **Sample** | **Flow Rate (sccm)** | **Contact Angle (°)** | | | **Surface Free Energy ($mJ \cdot m^{-2}$)** |
|---|---|---|---|---|---|
| | | Water | $CH_2I_2$ | Ethylene glycol | Total |
| 0. PET reference | / | 76 ± 1 | 27 ± 1 | 31 ± 1 | 46 |
| 1. ethyl lactate/PET | 250 | 67 ± 2 | 32 ± 1 | 36 ± 1 | 48 |
| 2. ethyl lactate/PET | 500 | 47 ± 1 | 33 ± 2 | 29 ± 1 | 55 |
| 3. ethyl lactate/PET | 750 | 38 ± 1 | 33 ± 2 | 25 ± 0 | 55 |
| 4. ethyl lactate/PET | 1000 | 27 ± 2 | 46 ± 2 | 29 ± 2 | 60 |
| 5. methyl lactate/PET | 250 | 67 ± 2 | 30 ± 3 | 27 ± 3 | 50 |
| 6. methyl lactate/PET | 500 | 60 ± 2 | 32 ± 1 | 36 ± 2 | 50 |
| 7. methyl lactate/PET | 750 | 57 ± 2 | 37 ± 2 | 23 ± 2 | 51 |

| | | | | | |
|---|---|---|---|---|---|
| 8. methyl lactate/PET | 1000 | 51 ± 3 | 48 ± 2 | 48 ± 1 | 50 |

### 3.3 Morphology of the tested materials

#### 3.3.1 Scanning electron microscopy

Figure 7 illustrates the surface morphology of PET in response to plasma treatment. Figure 7A presents a typical image of untreated PET film, characterized predominantly by the presence of irregular protrusions on the surface. In contrast, plasma-treated samples, depicted in Figures 7B and 7C, exhibit notable modifications in surface topography. Although some irregular protrusions remain visible following plasma treatment, the overall surface appears considerably smoother. Moreover, Figure 7C demonstrates an even greater degree of surface smoothness compared to the untreated PET, with only a few residual protrusions observed.

These findings suggest that a substantial number of micrometer-scale protrusions are effectively reduced or eliminated, a phenomenon that may be associated with the bombardment of the sample surface by energetic particles generated during the plasma treatment process [27].

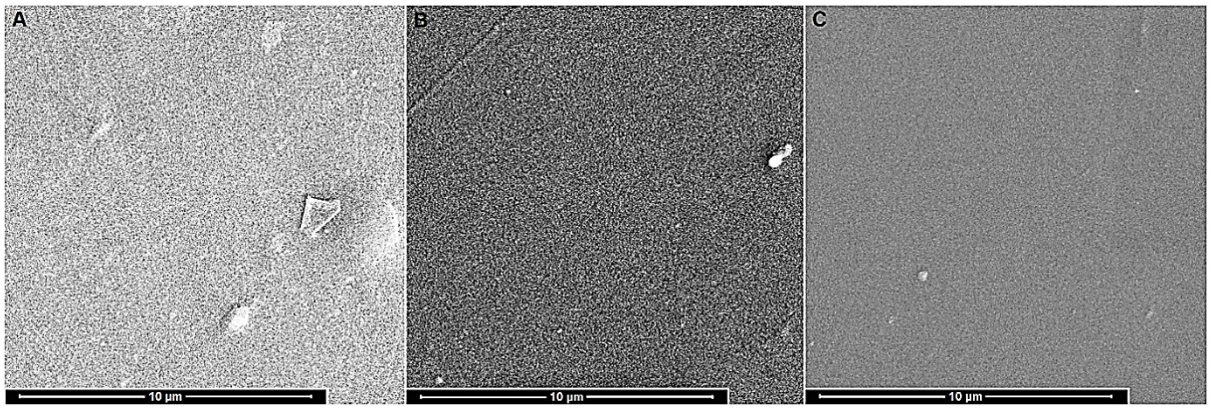


Figure 7: Representative SEM images of PET sample surfaces, obtained at approximately 10,000× magnification (scale bar: 10 µm), illustrating surface morphology variations: (A) untreated PET film, (B) ethyl lactate plasma-treated sample (nitrogen flow rate: 1000 sccm), and (C) methyl lactate plasma-treated sample (nitrogen flow rate: 1000 sccm).

#### 3.3.2 Atomic force microscopy

Figure 8 presents atomic force microscopy (AFM) images illustrating the surface topography of samples. The surface topography of a reference sample, untreated polyethylene terephthalate (PET) film, was analyzed using AFM in tapping mode. Similarly, the surface morphology of samples coated with plasma-prepared layers of methyl lactate/PET and ethyl lactate/PET was examined under identical conditions. The scanned surface area measured 2 × 2 µm. The images

on the left part of the figure depict three-dimensional representations of the individual samples, while the corresponding two-dimensional models are displayed on the right.

The untreated PET surface exhibits a heterogeneous morphology with relatively pronounced nanoscale undulations and irregular height fluctuations reaching approximately 60 nm. This morphology is typical for semi-crystalline PET films and reflects the coexistence of amorphous and crystalline domains formed during film processing. The root mean square roughness of pristine PET (Rq ≈ 2.6 nm) indicates a comparatively heterogeneous surface with locally exposed microstructural features [34].

Following plasma deposition, both modified samples show a substantial transformation of the original PET topography, confirming the formation of a continuous plasma-polymerized layer. The ethyl lactate/PET surface is characterized by a fine granular nanostructure composed of uniformly distributed nanoscale features, with height variations on the order of several nanometers and a reduced roughness (Rq ≈ 1.6 nm). This observation aligns with the findings of Milaniak et al., who reported that plasma polymerization of ethyl lactate results in a less pronounced surface roughness [35]. In contrast, the methyl lactate/PET sample displays a more homogeneous and smoother morphology with smaller, more compact nanoscale features, also exhibiting height variations on the order of several nanometers and a further reduction in roughness (Rq ≈ 0.6 nm). The smoother morphology suggests the formation of a denser and more uniform plasma polymer layer, which may be associated with differences in precursor fragmentation pathways and polymerization kinetics. Similar morphology evolution has been reported for plasma polymer films derived from oxygen-containing organic precursors, where film densification and uniform growth lead to reduced nanoscale roughness [18,19]

Overall, the quantitative AFM roughness values (Rq) decreased from 2.6 nm for untreated PET to 1.6 nm for ethyl lactate/PET and 0.6 nm for methyl lactate/PET, confirming progressive surface smoothing after plasma deposition. The combination of reduced roughness and increased surface polarity may promote the formation of stable hydration layers, which are known to influence wettability and bacterial adhesion [36].

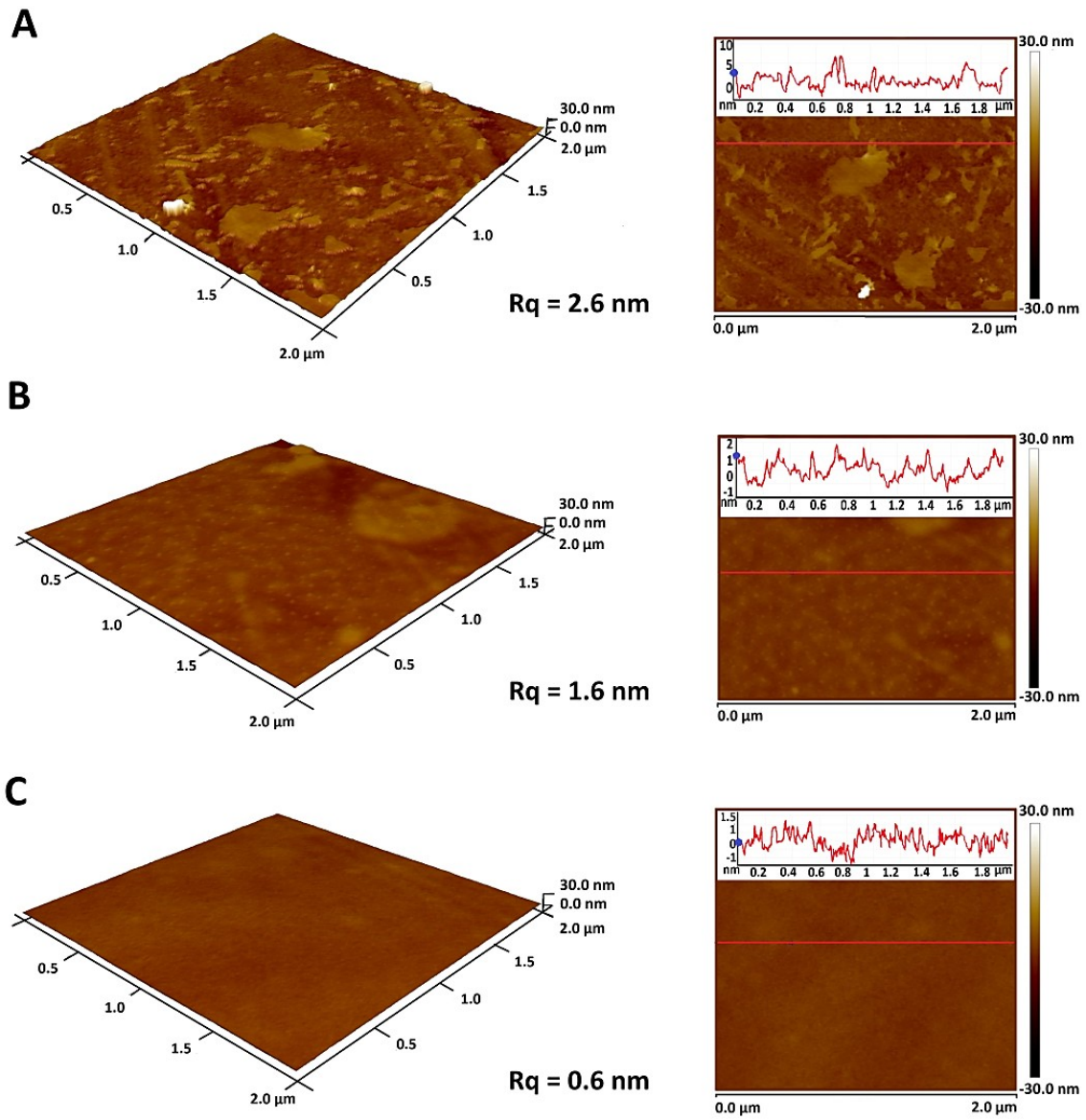


Figure 8: Atomic force microscopy (AFM) representations of the surface topography of samples: (A) untreated PET film, (B) ethyl lactate plasma-treated sample (flow rate 1000 sccm), and (C) methyl lactate plasma-treated sample (flow rate 1000 sccm), including corresponding surface roughness values (Rq).

### 3.4 Antibacterial properties of the tested materials

The antibacterial activity of the prepared films was evaluated in accordance with the international standard ISO 22196:2011 [15]. The assessment was conducted on sample films containing methyl lactate and ethyl lactate, using *E. coli* as a representative gram-negative bacterial strain and *S. aureus* as an example of gram-positive strain. As can be seen in Table 4,

samples with methyl lactate exhibit greater antimicrobial efficacy. Notably, sample 6, deposited at a flow rate of 500 sccm, demonstrated strong antibacterial activity (R = 3.4) against *E. coli* and significant activity (R = 2.1) against *S. aureus*. Furthermore, sample 5 has been found to be particularly relevant, as it exhibits significant antimicrobial properties against both tested bacterial strains.

The observed antibacterial behavior may be partially associated with the incorporation of nitrogen-containing functional groups, including amine-related species, as suggested by XPS analysis. Previous studies have reported that amine-containing surfaces can contribute to antibacterial effects and influence bacterial adhesion behavior [37],[38],[39]. In addition, Mentheour et al. demonstrated that antibacterial effects in plasma-treated systems may also be linked to enhanced hydrophilicity induced by reactive nitrogen species generated in dielectric barrier discharge plasma [40]. Therefore, the antibacterial performance observed in the present study is likely governed by a combination of increased surface hydrophilicity, hydration-layer formation, altered surface free energy, and nitrogen-containing surface functionalities rather than by a single dominant mechanism.

Interestingly, the strongest antibacterial activity was not observed for the samples exhibiting the highest hydrophilicity. In the case of methyl lactate-derived coatings, the most pronounced antibacterial performance was achieved at a precursor flow rate of 500 sccm, whereas the lowest water contact angle was obtained at 1000 sccm. This observation suggests that antibacterial behavior is not governed solely by wettability, but rather by a complex interplay of surface physicochemical properties. Besides hydrophilicity, factors such as the density and distribution of nitrogen-containing functional groups, surface free energy balance, hydration-layer stability, and coating structure may significantly influence bacterial adhesion and survival. Furthermore, variations in precursor flow rate can affect plasma fragmentation pathways and deposition kinetics, potentially leading to differences in coating cross-linking and surface chemistry. Therefore, an optimal antibacterial response may arise from a balanced combination of surface properties rather than from maximum hydrophilicity alone, which is consistent with previous studies demonstrating that bacterial adhesion is governed by the combined effects of wettability, surface chemistry, surface free energy, and interfacial interactions [36],[41],[42].

In general, surfaces exhibiting moderate wettability tend to facilitate bacterial or cellular adhesion more effectively than surfaces that are either highly hydrophobic or extremely hydrophilic. Additionally, an increase in surface free energy (Table 3), particularly in its polar or acid-base components, along with an enhancement of the electron donor character of the

substrate, has been shown to reduce bacterial adhesion [36,43]. The bacterial-repellent behavior of highly hydrophilic surfaces is frequently associated with the formation of hydration layers at the solid–liquid interface, which may reduce nonspecific adsorption of proteins and inhibit bacterial attachment [40].

Surface roughness is another important factor affecting bacterial adhesion, as it influences surface area and interfacial interactions between the material and bacterial cells. This reduction in shear force helps prevent the detachment of adhered bacteria [43]. However, nanoscale surface roughness has been found to exhibit the most effective anti-adhesion properties, whereas microscale roughness tends to promote bacterial adhesion. In contrast, smooth surfaces influence bacterial behaviour primarily through other material properties, such as surface chemistry and surface energy [36].

Considering the relatively thin nature of the plasma-deposited layers, as suggested by ATR-FTIR analysis, further investigation of coating durability, aging behavior, adhesion stability, and long-term retention of hydrophilic and antibacterial properties will be necessary for future practical applications. The durability of the antibacterial effect was subsequently evaluated after one year of aging and is discussed in Section 3.5.

Table 4 Antibacterial activity (R) of films containing methyl lactate and ethyl lactate, deposited at varying monomer flow rates, against gram-positive and gram-negative bacterial strains after 24 hours of incubation.

| **Samples** | ***Staphylococcus aureus* CCM 4516** | | ***Escherichia coli* CCM 4517** | |
|---|---|---|---|---|
| | **$N_x$(CFU·cm$^{-2}$)** | **R** | **$N_x$(CFU·cm$^{-2}$)** | **R** |
| 0. PET reference | $2.4\times10^{5}$ | $U_t$ = 5.4±0.2 | $1.6\times10^{6}$ | $U_t$ = 6.2±0.2 |
| 1. ethyl lactate/PET | $1.0\times10^{5}$ | 0.4±0.0 | $4.3\times10^{5}$ | 0.6±0.1 |
| 2. ethyl lactate/PET | $2.6\times10^{4}$ | 1.0±0.2 | $2.9\times10^{5}$ | 0.7±0.1 |
| 3. ethyl lactate/PET | $6.8\times10^{4}$ | 0.5±0.0 | $1.5\times10^{5}$ | 1.1±0.0 |
| 4. ethyl lactate/PET | $3.1\times10^{4}$ | 0.9±0.1 | $3.9\times10^{5}$ | 0.6±0.0 |
| 5. methyl lactate/PET | $1.2\times10^{3}$ | 2.3±0.1 | $1.7\times10^{4}$ | 2.0±0.0 |
| 6. methyl lactate/PET | $1.9\times10^{3}$ | 2.1±0.1 | $6.5\times10^{2}$ | 3.4±0.1 |
| 7. methyl lactate/PET | $6.1\times10^{4}$ | 0.6±0.0 | $4.2\times10^{5}$ | 0.6±0.0 |
| 8. methyl lactate/PET | $9.2\times10^{4}$ | 0.4±0.0 | $2.8\times10^{5}$ | 0.8±0.2 |

### 3.5 Aging stability of antibacterial properties

To address the durability of the antibacterial effect, the coated PET films were re-tested after one year of aging using the same ISO 22196-based procedure, and the results are summarized in Table 5. Since the initial and aged samples were evaluated in independent antibacterial assays, the comparison was based primarily on the antibacterial activity values (R), which are normalized to the corresponding PET reference within each experiment. Direct comparison of absolute CFU·cm$^{-2}$ values should therefore be interpreted with caution. Nevertheless, the low standard deviations of the R values indicate good repeatability within each individual assay (Table 5).

Table 5 Durability of antibacterial properties after one year of aging.

| **Samples** | ***Staphylococcus aureus* CCM 4516** | | ***Escherichia coli* CCM 4517** | |
|---|---|---|---|---|
| | **$N_x$(CFU·cm$^{-2}$)** | **R** | **$N_x$(CFU·cm$^{-2}$)** | **R** |
| 0. PET reference | 3.5x10$^5$ | $U_t$ = 5.5±0.1 | 2.0x10$^4$ | $U_t$ = 4.3±0.5 |
| 1. ethyl lactate/PET | 1.2x10$^5$ | 0.4±0.1 | 1.2x10$^3$ | 1.2±0.0 |
| 2. ethyl lactate/PET | 3.5x10$^5$ | 0.0±0.0 | 4.0x10$^3$ | 0.7±0.1 |
| 3. ethyl lactate/PET | 3.7x10$^5$ | 0.0±0.0 | 6.9x10$^2$ | 1.5±0.0 |
| 4. ethyl lactate/PET | 3.5x10$^5$ | 0.0±0.0 | 1.8x10$^3$ | 1.0±0.0 |
| 5. methyl lactate/PET | 3.3x10$^3$ | 2.0±0.1 | 1.6x10$^1$ | 3.1±0.0 |
| 6. methyl lactate/PET | 1.1x10$^5$ | 0.4±0.2 | 7.5x10$^0$ | 3.3±0.3 |
| 7. methyl lactate/PET | 1.9x10$^5$ | 0.2±0.1 | 1.2x10$^3$ | 1.2±0.1 |
| 8. methyl lactate/PET | 2.5x10$^5$ | 0.1±0.0 | 1.1x10$^3$ | 1.3±0.1 |

After one year of aging, the antibacterial performance showed a clear dependence on both the plasma precursor and the bacterial strain. Ethyl lactate-derived coatings exhibited only limited antibacterial activity after aging, particularly against *S. aureus*. In contrast, selected methyl lactate-derived coatings retained substantial antibacterial activity. Sample 5 maintained significant activity against both tested strains (R = 2.0 ± 0.1 for *S. aureus* and R = 3.1 ± 0.0 for *E. coli*), while sample 6 preserved strong activity against *E. coli* (R = 3.3 ± 0.3), although its activity against *S. aureus* decreased considerably.

The partial decrease in antibacterial activity after aging may be associated with well-known aging phenomena reported for plasma-modified polymer surfaces, including surface reorganization, hydrophobic recovery, and partial loss or reorientation of polar functional groups.

Overall, the aging study demonstrates that the antibacterial functionality of the plasma-polymerized coatings was partially retained after one year of storage. The durability of the antibacterial effect was dependent on both the coating composition and the bacterial strain. The most balanced long-term performance was observed for the methyl lactate-derived coating deposited at 500 sccm (sample 5), which retained antibacterial activity against both Gram-positive and Gram-negative bacteria.

## 4 Conclusion

In this study, lactate esters were obtained through the model chemical recycling of a biopolymer and subsequently modified via plasma deposition. This process enabled the development of a method for depositing antibacterial films on PET surfaces.

ATR-FTIR spectroscopy indicated the presence of O–H bonds may contribute to the enhanced hydrophilicity of the samples, particularly in the ethyl lactate-based coating. Complementary insights were provided by XPS analysis, which revealed the formation of oxygen- and nitrogen-containing functional groups, with C=O, C–N, and N–C=O bonds being most pronounced in the ethyl lactate/PET sample. Considering that XPS probes only the top ~5–10 nm of the surface, whereas ATR-FTIR provides information from depths up to the micrometer scale, the combined use of these techniques enables a comprehensive evaluation of both surface-specific and bulk-like chemical characteristics. Spectroscopic ellipsometry confirmed the successful deposition of thin plasma-polymerized coatings with thicknesses ranging from approximately 60 to 93 nm, depending on the precursor type and flow rate. The combined results of XPS, contact angle measurements, SEM, AFM analyses and spectroscopic ellipsometry consistently indicate the formation of thin plasma-polymerized surface layers on PET substrates. The strong contribution of the PET substrate observed in ATR-FTIR spectra further suggests that the deposited coatings are relatively thin. Future work will focus on evaluation of coating uniformity, cross-linking characteristics, and long-term stability.

The chemical composition and surface morphology analyses revealed significant differences in topography between plasma-treated and untreated samples. Notably, the plasma-treated films exhibited antibacterial properties against both *S. aureus* and *E. coli* in comparison to untreated

PET film. This antibacterial effect may be associated with enhanced hydrophilicity and nitrogen-containing functionalities.

The one-year aging study demonstrated that the antibacterial performance was partially retained after storage under ambient laboratory conditions, indicating a degree of long-term stability of the plasma-treated surfaces. In particular, selected methyl lactate-derived coatings maintained substantial antibacterial activity after aging, highlighting their potential for applications requiring durable antibacterial functionality.

The present study demonstrates the feasibility of utilizing lactate esters prepared from virgin PLA through model chemical recycling experiments as unconventional plasma precursors for functional surface coatings. Although the precursors were not obtained from real post-consumer PLA waste streams, the work provides proof-of-concept for future integration of chemically recycled PLA-derived compounds into plasma-based surface engineering strategies within a circular economy framework.

## CRediT authorship contribution statement

Monika Strašáková: Writing – original draft, Visualization, Validation, Methodology, Investigation, Data curation, Conceptualization. Eva Domincová Bergerová: Project administration, Methodology, Investigation, Conceptualization, Marián Lehocký: Methodology, Investigation. Veronika Hanuliak: Methodology, Investigation. Hana Pištěková: Methodology, Investigation. Michal Urbánek: Methodology, Investigation. Pavel Šťahel: Methodology, Investigation. Monika Stupavská: Methodology, Investigation. Jakub Klaban: Methodology, Investigation. Anežka Lengálová: Writing – review & editing. Vladimír Sedlařík: Supervision, Funding acquisition, Formal analysis.

## Declaration of competing interest

The authors declare that they have no conflict of interest.

## Acknowledgements

This work was supported from the European Just Transition Fund within the Operational Programme: Just Transition under the aegis of the Ministry of the Environment of the Czech Republic, project CirkArena number CZ.10.03.01/00/22_003/0000045 and the Ministry of

Education Youth and Sports of the Czech Republic, Operational Programme Johannes Amos Comenius OP JAC "Application potential development in the field of polymer materials in the context of circular economy compliance (POCEK)", number CZ.02.01.01/00/23_021/0009004. Authors are further grateful for co-funding from the development process of Centre of Polymer Systems, Tomas Bata University in Zlin, program DKRVO (RP/CPS/2024-28/002), (RP/CPS/2024-28/005), (RP/CPS/2024-28/007) and the Internal Grant Agency of the Centre of Polymer Systems in Zlin (IGA/CPS/2025/002) supported by the Ministry of Education Youth and Sports of the Czech Republic. One of the authors, M. Stupavská, gratefully acknowledges financial support from the Ministry of Education, Youth, and Sports of the Czech Republic under project LM2023039.

## Data availability

Data will be made available on request.

## References

[1] World Economic Forum, Ellen MacArthur Foundation and McKinsey & Company, The New Plastics Economy: Rethinking the future of plastics, 2016.

[2] R. Geyer, J.R. Jambeck, K.L. Law, Production, use, and fate of all plastics ever made, Sci. Adv. 3 (2017). https://doi.org/10.1126/SCIADV.1700782/SUPPL_FILE/1700782_SM.PDF.

[3] P. Majgaonkar, R. Hanich, F. Malz, R. Brüll, Chemical Recycling of Post-Consumer PLA Waste for Sustainable Production of Ethyl Lactate, Chemical Engineering Journal 423 (2021) 129952. https://doi.org/10.1016/J.CEJ.2021.129952.

[4] I.S. Bayer, S. Guzman-Puyol, J.A. Heredia-Guerrero, L. Ceseracciu, F. Pignatelli, R. Ruffilli, R. Cingolani, A. Athanassiou, Direct transformation of edible vegetable waste into bioplastics, Macromolecules 47 (2014) 5135–5143. https://doi.org/10.1021/MA5008557.

[5] M.N. Siddiqui, H.H. Redhwi, A.A. Al-Arfaj, D.S. Achilias, M.N.; Siddiqui, H.H.; Redhwi, A.A.; Al-Arfaj, D.S. Achilias, Chemical Recycling of PET in the Presence of the Bio-Based Polymers, PLA, PHB and PEF: A Review, (2021). https://doi.org/10.3390/su131910528.

[6] A. Carné Sánchez, S.R. Collinson, The selective recycling of mixed plastic waste of polylactic acid and polyethylene terephthalate by control of process conditions, Eur. Polym. J. 47 (2011) 1970–1976. https://doi.org/10.1016/J.EURPOLYMJ.2011.07.013.

[75] H. Biederman, Plasma Polymer Films, Plasma Polymer Films (2004). https://doi.org/10.1142/P336.

[85] R. Chakraborty, A. Govind Anoop, A. Thakur, G. Chandra Mohanta, P. Kumar, Strategies To Modify the Surface and Bulk Properties of 3D-Printed Solid Scaffolds for Tissue Engineering Applications, 8 (2023) 5139–5156. https://doi.org/10.1021/acsomega.2c05984.

[95] N. Milaniak, G. Laroche, F. Massines, Atmospheric-pressure plasma-enhanced chemical vapor deposition of nanocomposite thin films from ethyl lactate and silica nanoparticles, Plasma Processes and Polymers 18 (2021) 2000153. https://doi.org/10.1002/PPAP.202000153.

[160] B. Nisol, F. Reniers, Challenges in the characterization of plasma polymers using XPS, J. Electron Spectros. Relat. Phenomena 200 (2015) 311–331. https://doi.org/10.1016/J.ELSPEC.2015.05.002.

[163] M. Laurent, E. Desjardins, M. Meichelboeck, N. Naudé, L. Stafford, N. Gherardi, G. Laroche, Characterization of argon dielectric barrier discharges applied to ethyl lactate plasma polymerization, J. Phys. D Appl. Phys. 50 (2017) 475205. https://doi.org/10.1088/1361-6463/AA916D.

[167] E.D. Bergerova, M. Strasakova, J. Cisar, T. Sopik, M. Dusankova, I. Vincent, J. Klaban, D. Hanusova, S. Uhercova, L. Hanykova, V. Sedlarik, Impact of solvolysis on the decomposition efficiency of poly(lactic acid) materials with insight into their non-uniform architecture, Int. J. Biol. Macromol. 302 (2025) 140529. https://doi.org/10.1016/J.IJBIOMAC.2025.140529.

[171] P. St'ahel, V. Mazánková, D. Podzemná, E. Podzemná, V. Pizúrová, J. Jurmanová, L. Prokeš, M. Lehocký, K. Ozaltin, H. Pištěková, D. Trunec, Antibacterial Thin Films Deposited from Propane-Butane Mixture in Atmospheric Pressure Discharge, (2023). https://doi.org/10.3390/ijms24021706.

[175] D.K. Owens, R.C. Wendt, Estimation of the surface free energy of polymers, J. Appl. Polym. Sci. 13 (1969) 1741–1747. https://doi.org/10.1002/APP.1969.070130815.

[177] ISO 22196:2011 - Measurement of antibacterial activity on plastics and other non-porous surfaces, (n.d.). https://www.iso.org/standard/54431.html (accessed April 15, 2024).

[179] J.C.-E. of analytical chemistry, undefined 2000, Interpretation of infrared spectra, a practical approach, Researchgate.NetJ CoatesEncyclopedia of Analytical Chemistry, 2000•researchgate.Net (n.d.) 10815–10837. https://www.researchgate.net/profile/Chandana-

Chandrasekher/post/How-to-interpret-my-FTIR-spectrum-Is-there-any-online-software-available-to-interpret-the-spectrum/attachment/5ac4a7094cde260d15d6bc94/AS%3A611637941780481%401522837257071/download/joan+coates.pdf (accessed May 2, 2024).

[187] K. Štěpánková, M. Müllerová, Š. Žídek, H. Pištěková, P. Urbánek, P. Sťahel, D. Trunec, A. Popelka, N. Kallingal, M. Mozetič, M. Lehocky, Plasma Polymerization of Pentane and Hexane for Antibacterial and Biocompatible Thin Films, Plasma Processes and Polymers (2025) e2400266. https://doi.org/10.1002/PPAP.202400266.

[190] M. Laurent, E. Desjardins, M. Meichelboeck, N. Naudé, L. Stafford, N. Gherardi, G. Laroche, M. Laurent, E. Desjardins, M. Meichelboeck, N. Naudé, L. Stafford, N. Gherardi, G. Laroche, Characterization of argon dielectric barrier discharges applied to ethyl lactate plasma polymerization, JPhD 50 (2017) 475205. https://doi.org/10.1088/1361-6463/AA916D.

[194] F. Massines, N. Gherardi, N. Naudé, P. Ségur, Recent advances in the understanding of homogeneous dielectric barrier discharges, The European Physical Journal Applied Physics 47 (2009). https://doi.org/10.1051/EPJAP/2009064.

[197] C. Contini, M.G. Katsikogianni, F.T. O'Neill, M. O'Sullivan, F. Boland, D.P. Dowling, F.J. Monahan, Storage Stability of an Antioxidant Active Packaging Coated with Citrus Extract Following a Plasma Jet Pretreatment, Food Bioproc. Tech. 7 (2014) 2228–2240. https://doi.org/10.1007/S11947-013-1210-9/FIGURES/7.

[201] A. Vesel, M. Mozetic, Modification of PET surface by nitrogen plasma treatment, J. Phys. Conf. Ser. 100 (2008). https://doi.org/10.1088/1742-6596/100/1/012027.

[203] P.M. Dietrich, S. Bahr, T. Yamamoto, M. Meyer, A. Thissen, Chemical surface analysis on materials and devices under functional conditions – Environmental photoelectron spectroscopy as non-destructive tool for routine characterization, J. Electron Spectros. Relat. Phenomena 231 (2019) 118–126. https://doi.org/10.1016/J.ELSPEC.2017.12.007.

[207] J.W. Pinder, G.H. Major, D.R. Baer, J. Terry, J.E. Whitten, J. Čechal, J.D. Crossman, A.J. Lizarbe, S. Jafari, C.D. Easton, J. Baltrusaitis, M.A. van Spronsen, M.R. Linford, Avoiding common errors in X-ray photoelectron spectroscopy data collection and analysis, and properly reporting instrument parameters, Applied Surface Science Advances 19 (2024) 100534. https://doi.org/10.1016/J.APSADV.2023.100534.

[24] A. Szczurek, T.N.L. Tran, J. Kubacki, A. Gąsiorek, K. Startek, A. Mazur-Nowacka, R. Dell'Anna, C. Armellini, S. Varas, A. Carlotto, A. Chiasera, A. Łukowiak, J. Krzak, M. Ferrari, Polyethylene terephthalate (PET) optical properties deterioration induced by temperature and protective effect of organically modified SiO2–TiO2 coating, Mater. Chem. Phys. 306 (2023) 128016. https://doi.org/10.1016/J.MATCHEMPHYS.2023.128016.

[25] S.M. Pelagade, N.L. Singh, A. Qureshi, R.S. Rane, S. Mukherjee, U.P. Deshpande, V. Ganesan, T. Shripathi, Investigation of surface properties of Ar-plasma treated polyethylene terephthalate (PET) films, Nucl. Instrum. Methods Phys. Res. B 289 (2012) 34–38. https://doi.org/10.1016/J.NIMB.2012.08.010.

[26] X. Zhang, L. Wang, E. Levänen, Superhydrophobic surfaces for the reduction of bacterial adhesion, RSC Adv. 3 (2013) 12003–12020. https://doi.org/10.1039/C3RA40497H.

[27] J. Lai, B. Sunderland, J. Xue, S. Yan, W. Zhao, M. Folkard, B.D. Michael, Y. Wang, Study on hydrophilicity of polymer surfaces improved by plasma treatment, Appl. Surf. Sci. 252 (2006) 3375–3379. https://doi.org/10.1016/J.APSUSC.2005.05.038.

[28] E.E. Johnston, B.D. Ratner, Surface characterization of plasma deposited organic thin films, J. Electron Spectros. Relat. Phenomena 81 (1996) 303–317. https://doi.org/10.1016/0368-2048(95)02666-5.

[29] N.Y. Cui, N.M.D. Brown, Modification of the surface properties of a polypropylene (PP) film using an air dielectric barrier discharge plasma, Appl. Surf. Sci. 189 (2002) 31–38. https://doi.org/10.1016/S0169-4332(01)01035-2.

[30] H. Dvořáková, J. Čech, M. Stupavská, L. Prokeš, J. Jurmanová, V. Buršíková, J. Ráheľ, P. Sťahel, H. Dvořáková, J. Čech, M. Stupavská, L. Prokeš, J. Jurmanová, V. Buršíková, J. Ráheľ, P. Sťahel, Fast Surface Hydrophilization via Atmospheric Pressure Plasma Polymerization for Biological and Technical Applications, Polymers 2019, Vol. 11, 11 (2019). https://doi.org/10.3390/POLYM11101613.

[31] M. Keil, C.S. Rastomjee, A. Rajagopal, H. Sotobayashi, A.M. Bradshaw, C.L.A. Lamont, D. Gador, C. Buchberger, R. Fink, E. Umbach, Argon plasma-induced modifications at the surface of polycarbonate thin films, Appl. Surf. Sci. 125 (1998) 273–286. https://doi.org/10.1016/S0169-4332(97)00501-1.

[341] N. Sakudo, D. Mizutani, Y. Ohmura, H. Endo, R. Yoneda, N. Ikenaga, H. Takikawa, Surface modification of PET film by plasma-based ion implantation, Nucl. Instrum. Methods Phys. Res. B 206 (2003) 687–690. https://doi.org/10.1016/S0168-583X(03)00824-3.

[344] M. Toufik, A. Mas, V. Shkinev, A. Nechaev, A. Elharfi, F. Schué, Improvement of performances of PET track membranes by plasma treatment, Eur. Polym. J. 38 (2002) 203–209. https://doi.org/10.1016/S0014-3057(01)00130-6.

[347] A. Vesel, M. Mozetic, Modification of PET surface by nitrogen plasma treatment, J. Phys. Conf. Ser. 100 (2008). https://doi.org/10.1088/1742-6596/100/1/012027.

[349] N. Milaniak, G. Laroche, F. Massines, Atmospheric-pressure plasma-enhanced chemical vapor deposition of nanocomposite thin films from ethyl lactate and silica nanoparticles, Plasma Processes and Polymers 18 (2021) 2000153. https://doi.org/10.1002/PPAP.202000153.

[352] Y. Yuan, M.P. Hays, P.R. Hardwidge, J. Kim, Surface characteristics influencing bacterial adhesion to polymeric substrates, RSC Adv. 7 (2017) 14254–14261. https://doi.org/10.1039/C7RA01571B.

[355] Y. Endo, T. Tani, M. Kodama, Antimicrobial activity of tertiary amine covalently bonded to a polystyrene fiber., Appl. Environ. Microbiol. 53 (1987) 2050. https://doi.org/10.1128/AEM.53.9.2050-2055.1987.

[358] V. Baidin, T.W. Owens, M.B. Lazarus, D. Kahne, Simple Secondary Amines Inhibit Growth of Gram-Negative Bacteria through Highly Selective Binding to Phenylalanyl-tRNA Synthetase, J. Am. Chem. Soc. 143 (2021) 623–627. https://doi.org/10.1021/JACS.0C11113/ASSET/IMAGES/LARGE/JA0C11113_0004.JPEG.

[362] H. Dvořáková, J. Čech, M. Stupavská, L. Prokeš, J. Jurmanová, V. Buršíková, J. Ráhel', P. St'ahel, Fast Surface Hydrophilization via Atmospheric Pressure Plasma Polymerization for Biological and Technical Applications, Polymers 2019, Vol. 11, Page 1613 11 (2019) 1613. https://doi.org/10.3390/POLYM11101613.

[366] R. Mentheour, Z. Machala, Coupled Antibacterial Effects of Plasma-Activated Water and Pulsed Electric Field, Front. Phys. 10 (2022). https://doi.org/10.3389/FPHY.2022.895813/FULL.

[369] S. Zheng, M. Bawazir, A. Dhall, H.E. Kim, L. He, J. Heo, G. Hwang, Implication of Surface Properties, Bacterial Motility, and Hydrodynamic Conditions on Bacterial Surface Sensing and

Their Initial Adhesion, Front. Bioeng. Biotechnol. 9 (2021) 643722. https://doi.org/10.3389/FBIOE.2021.643722/BIBTEX.

[42] X. Zhang, L. Wang, E. Levänen, Superhydrophobic surfaces for the reduction of bacterial adhesion, RSC Adv. 3 (2013) 12003–12020. https://doi.org/10.1039/C3RA40497H.

[43] S. Zheng, M. Bawazir, A. Dhall, H.E. Kim, L. He, J. Heo, G. Hwang, Implication of Surface Properties, Bacterial Motility, and Hydrodynamic Conditions on Bacterial Surface Sensing and Their Initial Adhesion, Front. Bioeng. Biotechnol. 9 (2021) 643722. https://doi.org/10.3389/FBIOE.2021.643722/BIBTEX.